Macromolecules
ARTICLE

Macromolecules **2010**, *43*, 4727–4732 **4727**
DOI: 10.1021/ma100303d

Two Lamellar to Fibrillar Transitions in the Tensile Deformation of High-Density Polyethylene

Zhiyong Jiang,[†,⊥] Yujing Tang,[†,⊥] Jens Rieger,[‡,⊥] Hans-Friedrich Enderle,[§,⊥] Dieter Lilge,[§,⊥] Stephan V. Roth,[∥,⊥] Rainer Gehrke,[∥,⊥] Walter Heckmann,[‡,⊥] and Yongfeng Men*[,†]

[†]*State Key Laboratory of Polymer Physics and Chemistry, Changchun Institute of Applied Chemistry, Chinese Academy of Sciences, Renmin Street 5625, 130022 Changchun, People's Republic of China,* [‡]*BASF SE, Polymer Research, 67056 Ludwigshafen, Germany,* [§]*Basell Polyolefine GmbH, R&D, 65926 Frankfurt, Germany, and* [∥]*HASYLAB am DESY, Notkestrasse 85, 22607 Hamburg, Germany.* [⊥]*E-mail addresses: (Z.Y.J.) jiangzhy@ciac.jl.cn; (Y.J.T.) tangyj@ciac.jl.cn; (J.R.) jens.rieger@basf.com; (H.-F.E.) hans-friedrich.enderle@basell.com; (D.L.) dieter.lilge@basell.com; (S.V.R.) stephan.roth@desy.de; (R.G.) rainer.gehrke@desy.de; (W.H.) walter.heckmann@basf.com.*

Received February 8, 2010; Revised Manuscript Received April 9, 2010

ABSTRACT: The structural evolution of tensile-deformed high-density polyethylene (HDPE) at the lamellar level was investigated as a function of strain using a scanning synchrotron small-angle X-ray scattering technique. Intralamellar crystalline block slips were activated at small deformations, whereas stress-induced fragmentation and recrystallization process proceeded at a larger strain, yielding lamellae with polymeric chains preferentially oriented along the stretching direction. The critical strains marking the onset of the destruction of original crystallites and the fibril formation for isothermally crystallized HDPE were at about 0.4 and 1.2, respectively. In the case of a quenched sample, the critical strain was 0.4. In the isothermally crystallized sample two critical values were observed that could be traced back to the existence of two populations of lamellar stacks with significantly different interlamellar amorphous phase thicknesses. This resulted in distinct mobilities of the amorphous domains and, therefore, different moduli of the entangled amorphous networks. Consequently, the strain required to produce the critical network stress, which gave rise to a fragmentation of the crystalline blocks, was different for each stack of crystalline lamellae.

1. Introduction

Deformation behavior and tensile properties are very important characteristics of semicrystalline polymers that exhibit a nanoscopic layered structure consisting of crystalline lamellae and an amorphous phase.[1] Consequently, the tensile deformation of semicrystalline polymers has been extensively studied.[2−10] In particular, high-density polyethylene (HDPE) can serve as a model for semicrystalline polymers because of its simple chemical structure and interesting mechanical performance. Tensile stretching transforms the original microscopic spherulitic morphology into a highly oriented fibrillar one, where polymeric chains are preferentially aligned along the drawing direction.[11−16] However, the structural and molecular parameters involved in the deformation process is not yet completely understood, mainly because of the lack of structural and morphological information at the molecular and nanometric length scales during deformation. It is therefore essential to probe into the micro- and nanostructural changes, which occur during the mechanical deformation of the material, to gain further insight into the molecular mechanisms of deformation in initially isotropic PE and to provide possible routes for improvement of the material.[17−23] Two distinct arguments have been proposed in literature to account for the plastic nature underlying the lamellar to fibrillar transition. First, it is suggested that the deformation is accomplished by slips within the lamellae, including crystallographic fine slips and intralamellar mosaic block slips.[6,11,24−27] Second, stress-induced melting and recrystallization is proposed to be responsible for the change of the morphology during the deformation process.[28−31] Experimental evidence for both arguments has been extensively reported, including microscopic and X-ray diffraction investigations supporting the slip mechanism[8,12,24] and small-angle X-ray scattering (SAXS) experiments favoring the melting-recrystallization mechanism.[32−34]

Because they are composed of periodically stacked lamellar crystals with entangled amorphous polymeric chains in between, semicrystalline polymers exhibit a complex deformation behavior under tensile stress. The deformation is affected by the response of both the crystalline and the amorphous phase. However, the relative weights of the two contributions change with increasing deformation.[2,3] In recent years, Strobl et al. have performed extensive studies on the deformation mechanisms of semicrystalline polymers by employing true stress−strain measurements at constant strain rate. The results revealed that the tensile deformation of semicrystalline polymers is strain-controlled and that the deformation mechanism changes at critical strains, which are crystallinity and temperature invariant.[1,21,35−39] The deformation mechanism changes from being block slip mediated into a disaggregation-recrystallization process at a critical value of strain. The position of the critical strain at this point depends on the interplay between the entanglement density in the amorphous phase and the stability of the crystal blocks.[15,36]

To a large extent, the mechanical properties of HDPE depend on its microstructure and morphology, which in turn is affected by the crystallization conditions.[2,3,40,41] Thus, our main objective is to assess the influence of the crystalline structure and phase morphology on the deformation behavior of HDPE by means of positional scanning synchrotron SAXS. For this purpose, we

*To whom correspondence should be addressed. E-mail: men@ciac.jl.cn.

Published on Web 04/27/2010

have limited our observations to one deformation temperature. Samples with different thermal history before tensile deformation can be obtained through controlled crystallization modes. In the present work, we study the microstructural evolution of isothermally crystallized HDPE at the nanoscale at different deformation ratios after stretching at a selected temperature of 100 °C. The observations are directly related to the mobility of the amorphous phase and thus the modulus of the entangled amorphous network.

2. Experimental Section

The HDPE used in this study was supplied by BASELL Polyolefine, Frankfurt, Germany. The molecular weights were $M_w = 3.24 \times 10^5$ g/mol and $M_n = 2.3 \times 10^4$ g/mol. The material was first compression-molded at 180 °C and held in its molten state for 5 min to erase any residual local orientation. The molten sheet was then quickly transferred to a thermostatted oil bath, which had been preset at a crystallization temperature of 128 °C. After completion of isothermal crystallization, the sample was slowly cooled down to room temperature yielding a plate with 2 mm thickness. A rectangular strip with a dimension of 20 × 70 mm^2 was cut from the plate and mounted on a stretching device in a heating chamber that was preheated to 100 °C. When the desired temperature (100 °C) in the heating chamber had been reequilibrated for 5 min, the strip was stretched at a constant crosshead speed of 10 mm/min until neck propagation occurred over a large portion of the sample. The sample was tensile deformed at 100 °C to avoid strain-whitening, caused by cavitations in the sample during deformation, that spoils the SAXS patterns due to the strongly enhanced electron density contrast between the cavitations and the surrounding polymeric matrix.[42] The drawn sample was not fixed at its two ends in the stretched state when it was taken out of the tensile machine. To accurately measure the strain of the deformed sample along the neck shoulder, an optical image of the sample was used for the measurement. Assuming a constant volume during elongation, the Hencky equation of the strain ε_H was used as a measure for the deformation. It is defined as

$$\varepsilon_H = 2 \ln \frac{b_0}{b} \quad (1)$$

where b_0 and b represent the widths of the undeformed and deformed areas located at specific spots on the sample.

Synchrotron SAXS measurements were performed at the beamline BW4 at HASYLAB, DESY, Hamburg, Germany. The energy of the X-ray radiation was 8.979 keV, resulting in a wavelength of 0.13808 nm. The size of the primary X-ray beam at the sample position was 0.4 × 0.4 mm^2. The prestretched sample was mounted onto a two-dimensional translational stage at the beamline with a sample to detector distance of 6987 mm. At this distance, the effective scattering vector q ($q = (4\pi \sin \theta)/\lambda$, where 2θ is the scattering angle and λ is the wavelength) range is 0.03−0.51 nm^{-1}. The primary X-ray beam was first positioned at the middle of the horizontally placed sample bar. The sample was then moved stepwise in such a way that the X-ray beam scanned over the neck shoulder at a step length of 0.5 mm covering a strain from 0.07 to 1.48 on a single sample. SAXS patterns were collected at every step within 120 s. The SAXS data were calibrated for background scattering and normalized with respect to the primary beam intensity. Changes in scattering intensity due to varying sample thickness were corrected by measuring the sample adsorption using the ionization chambers on both sides of the sample and applying the corresponding data correction.

To obtain further information on the samples subjected to different tensile deformation ratios differential scanning calorimetry (DSC) measurements were conducted on deformed samples having two extreme draw ratios. A DSC 2920 (TA Instruments), which had been calibrated for temperature and melting enthalpy by using indium as a standard, was used during the experiments with a heating rate of 10 K/min. The crystallinity was derived from integrating the DSC traces with respect to a baseline drawn as a tangent to the trace at temperatures of 40 and 150 °C and relating the derived heat to the melting enthalpy (293 J/g) of the hypothetical 100% crystalline polyethylene.[43]

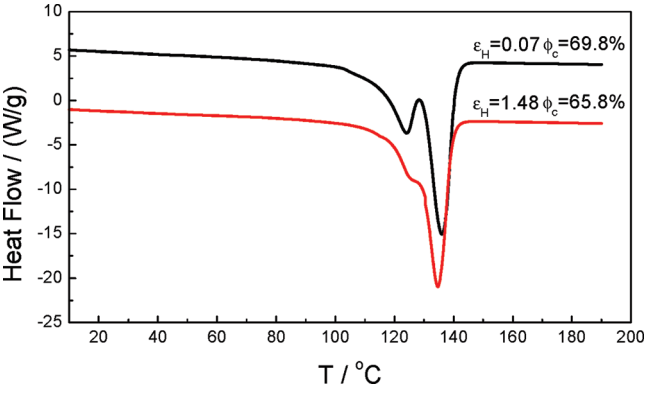

Figure 1. DSC melting curves of isothermally crystallized HDPE samples measured at a heating rate of 10 K/min after tensile deformation at 100 °C. The true strain and crystallinity are indicated on the graph.

To have a direct overview of the phase morphology of the isothermally crystallized HDPE sample transmission electron microscopy (TEM) measurements were conducted. For this, the HDPE sample was trimmed with a microtome to provide a trapezoidal block face shape. This sample was dipped in a solution of $RuCl_3$ in aqueous sodium hypochlorite for some hours and then ultramicrotomed at low temperatures with a Leica Ultracut S FCS.[44] The ultrathin sections had a thickness of about 80 nm. TEM was performed with a LEO 912 Omega using an acceleration voltage of 120 kV.

3. Results and Discussion

3.1. DSC and TEM Results. Before considering the microstructural evolution under tensile deformation, thermal analysis results are presented to provide insight into the influence of the crystallization mode and deformation ratio on the thermal behavior of the HDPE samples. Figure 1 shows the DSC melting curves of samples taken from un-necked parts and from the neck zones after having been elongated at 100 °C. Since plastic deformation already set in before the yield point, the un-necked region of the samples also exhibited several percentages of permanent deformation.[38,39] The values of the true strain (Figure 1) were derived from eq 1. Both melting curves of the isothermally crystallized HDPE samples display double endothermic peaks, indicating the existence of two populations of lamellar stacks with significantly different thermal stabilities. A double melting peak might also be caused by the occurrence of competing melting/crystallization processes but the scattering data discussed below substantiate the assumption that the former explanation for the double melting behavior holds. The crystallinity of the material decreased slightly after uniaxial elongation. This effect is due to the destruction of originally perfect lamellar crystallites and formation of defective crystals at the deformation temperature induced by mechanical treatment.

A natural question arising from the DSC data is how the two populations of lamellar stacks are arranged. To clarify this point, we present in Figure 2 TEM micrographs of the sample taken from the un-necked part. A global interpenetrating structure is observed in the top image with low magnification. Two populations of lamellar stacks with

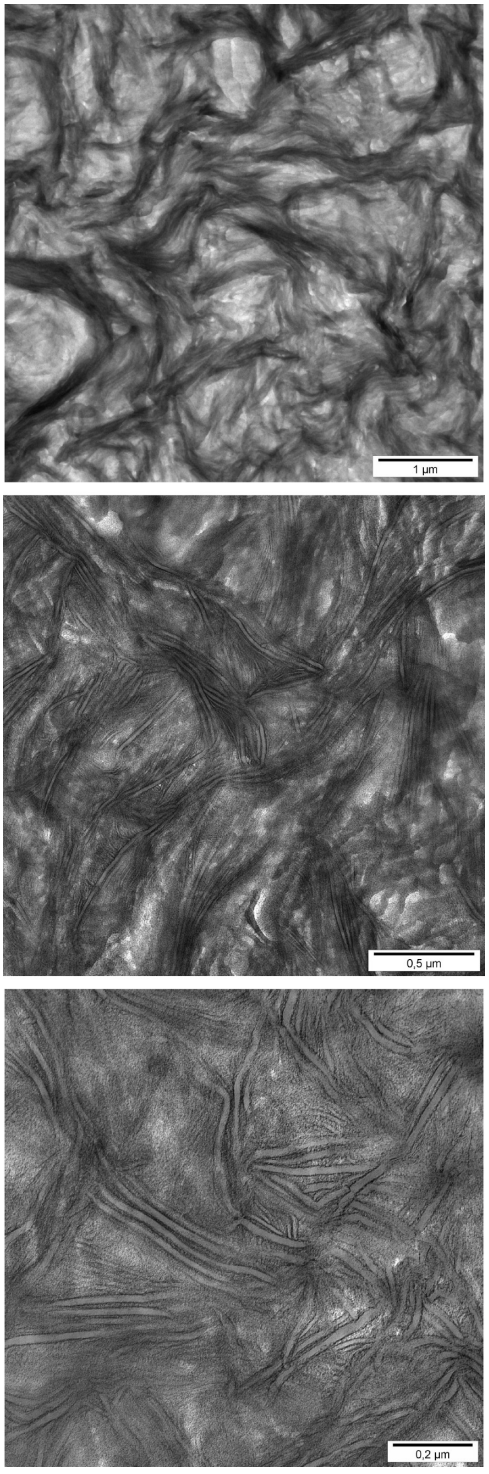

Figure 2. TEM micrographs of the isothermally crystallized HDPE sample taken from the un-necked region.

different crystalline lamellar thicknesses are clearly visible in images of higher magnifications (middle and bottom). Such a structure is due to the preparation procedure of first isothermal crystallization at a relatively high temperature of 128 °C and then cooling down to room temperature. Obviously, the sample was only able to crystallize to a limited extend after isothermal crystallization. During isothermal crystallization, only those chains having a sufficiently low number of defects (branches and chain-ends) can crystallize onto crystalline lamellae. Chains that are not able to crystallize during isothermal condition are repelled to the surrounding

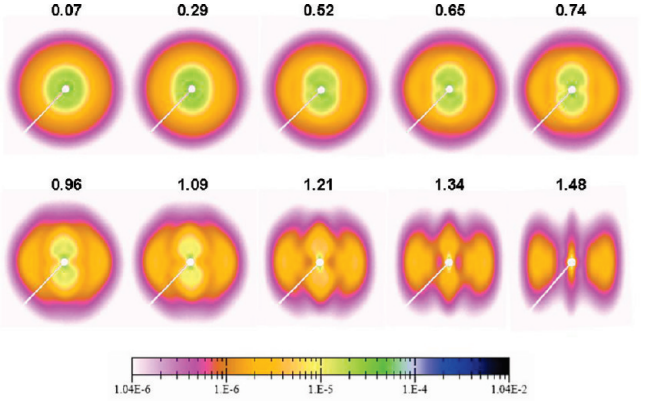

Figure 3. Selected small-angle X-ray scattering patterns of HDPE isothermally crystallized at 128 °C and tensile deformed at 100 °C as a function of true strain. The stretching direction is horizontal.

regions and crystallize at lower temperatures during cooling down yielding thinner lamellar crystallites. The structure observed in our system suggests a crystallization driven phase separation of polyethylene chains with different crystallization ability at isothermal condition. This implies that the behavior of the thicker lamellae in the current system must be similar to the one of linear polyethylene. For melt crystallized linear polyethylene, it is known that different secondary crystallization behavior showed up during cooling down depending on isothermal crystallization time.[45] New crystalline lamellae with reduced thickness would be created if the sample were cooled down after a short isothermal crystallization time whereas thickening of the existing lamellae occurred when the system was cooled down after prolonged isothermal crystallization.[45] Clearly, our system belongs to the latter case where well-organized stacks of thickened lamellae are observed. Polymer chains that cannot cocrystallize because of their higher content of defects are expelled from these stacks and form stacks of thinner lamellae at lower temperatures upon cooling the material.

3.2. SAXS Results. Information about changes in the lamellar structure during tensile deformation can be extracted directly from the 2D SAXS patterns. Selected SAXS patterns for isothermally crystallized HDPE samples, which had been deformed at 100 °C to different strains, are given in Figure 3. The SAXS patterns of the periodic lamellar structure of HDPE exhibit maxima at q_{max} when scanning along certain directions. The apparent value of the long spacing (d_{ac}) can be calculated using the Bragg equation

$$d_{ac} = \frac{2\pi}{q_{max}} \quad (2)$$

This long spacing d_{ac} is equal to the average thickness of a lamella together with one interlamellar amorphous layer measured along the lamellar normal. At this point of the data treatment, we did not take any symmetry considerations into account that might necessitate multiplication of the isotropic intensity value with q^2 (Lorentz correction). We are aware of the fact that this could lead to an error when comparing the d_{ac} values evaluated from isotropic and highly oriented samples. This point will be addressed below. As mentioned above, the un-necked region of the sample exhibited a macroscopic deformation of 0.07, which is also evident from the slight anisotropy of the respective scattering pattern.

The SAXS patterns for the isothermally crystallized sample collected at different strains exhibit two scattering

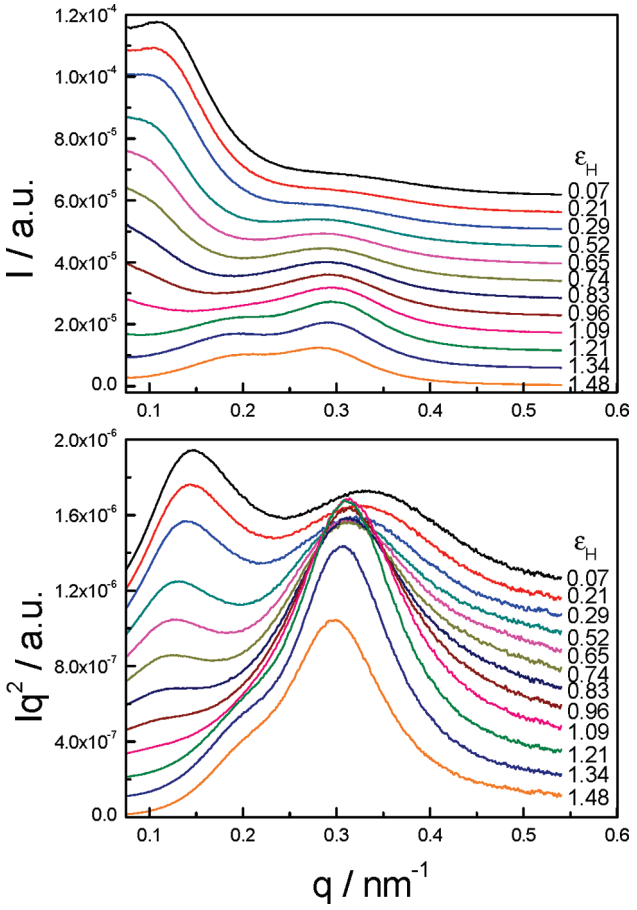

Figure 4. SAXS. One-dimensional scattering intensity distribution profiles for HDPE isothermally crystallized at 128 °C, taken along the stretching direction at different deformations. Peak positions were used to calculate the long spacing (d_{ac}).

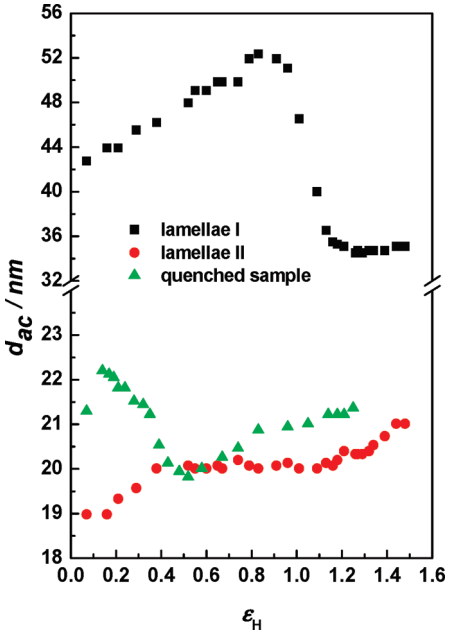

Figure 5. True-strain dependence of the long spacing d_{ac} along the drawing direction derived from Lorentz-corrected scattering curves. Lamellae I and lamellae II represent the thicker and thinner lamellar stacks in the isothermally crystallized HDPE sample.

intensity maxima (cf. Figure 4), reflecting the presence of two populations of lamellar stacks with different long spacing values. This finding supports the interpretation of DSC results given above. As the deformation ratio increases, the SAXS patterns transform from a scattering diagram with peaks perpendicular to the stretching direction at small deformations to a four-point scattering diagram at moderate strains and eventually to a highly anisotropic scattering intensity distribution with scattering peaks aligned in the meridional direction (i.e., along the stretching direction). The presence of four-point SAXS patterns is indicative of a slipping/tilting of the oriented lamellar crystallites. This observation can be explained by assuming that lamellar stacks that are inclined with respect to the macroscopic orientation direction are able to experience an intralamellar slip, keeping some correlation within the stacks, while lamellae with their normal parallel and perpendicular to the stretching direction are broken, resulting in a loss of SAXS intensity.

In an effort to further explain the evolution of the lamellar long spacing in the process of tensile deformation, the one-dimensional scattering intensity distributions along the stretching direction is considered (Figure 4). We took two approaches to represent the data of the isotropic samples with the correct q weighting; the scattering intensity was multiplied by q^2 for data processing (Lorentz correction) on the one hand, while for the data with fiber symmetry, that is, at high stretching ratios, no Lorentz correction was applied.[46,47] Clearly, both approaches are correct only for the respective extreme situations, where the lamellar stacks are distributed isotropically, that is, samples without strain, and where the stacks of lamellae are perfectly oriented with their normal along the drawing direction. In between these extremes, no unique recipe for data treatment is available because of the uneven distribution of scattered intensity in reciprocal space. Both sets of data are presented in Figure 4. Since two scattering peaks appear in the scattering intensity distributions of the isothermally crystallized sample, the profile was decomposed into contributions on the basis of two Gaussian functions. From the resulting fitted data the long spacing values for the sample after deformation measured along the stretching direction were calculated according to eq 2 (Figure 5). The evolution of the long spacing of the quenched sample, which was deformed at the same temperature, is also included in this figure. As pointed out in our previous investigations, for a semiquantitative discussion of the dependence of the long spacing on the strain, the type of data treatment (Lorentz correction versus no correction) only plays a minor role.[17,48] Consequently, in the present study the values of the long spacings were derived from the Lorentz-corrected scattering curves. Variations of the long spacing values along the stretching direction with strain exhibited a transition-like behavior for both samples (Figure 5). In the case of the isothermally crystallized sample, initially there is an increase in the long period due to stretching of the amorphous regions and possibly an accompanying slight rearrangement of lamellae. Subsequently a considerable drop in the long spacing from about 43 nm before necking to around 35 nm in the necked zone for thicker lamellar stacks (lamellae I) is observed. This behavior is in line with the assumption of a fragmentation and recrystallization process occurring during deformation. Since the imposed drawing temperature was lower than the isothermal crystallization temperature, the recrystallization process produces lamellae that are thinner than the original ones because of the high undercooling.[49] On the other hand, the long spacing of the thinner crystalline lamellae (lamellae II) increases by about 2 nm during deformation until it levels

off at a critical strain of 0.4. The long spacing of the quenched sample drops considerably up to a critical strain of 0.4 in the transition zone and then increases gradually with a further increase of the deformation ratio. It must be noted that the critical strain associated with the onset of the formation of fibrils, following the disaggregation of crystal blocks, is a true strain with a value of about 1.2 for lamellae I, whereas the critical value for lamellae II is 0.4, which is equivalent to the critical strain of the quenched sample. The further increase of the long period of lamellae II stacks above a strain of 1.2 is due to the combined deformation of reformed lamellae I and II stacks.

Finally, the physical situations at the two different critical strains are considered. Because of the interpenetrating nature of the structure built by the crystalline lamellae and the interlamellar entangled melt phase, the reaction of semicrystalline polymeric material upon stretching is affected by the behavior of both components. It is meanwhile accepted that the interplay between the state of the entangled amorphous phase and the intrinsic stability of the crystal blocks determines the position of the critical strain, at which the transition from slipping of the crystalline blocks to a fragmentation and recrystallization process occurs.[36] Since the crystalline lamellae are still persisting entities up to this point, the extension ratio at the transition point is directly related to the network modulus of the amorphous phase.[36] Thus, the critical strain reflects the property of the entangled amorphous phase. The average thickness of the amorphous and crystalline regions measured along the stretching direction can be evaluated from the one-dimensional electron density correlation function $K(z)$ as follows[1,45,50−52]

$$K(z) = \frac{\int_0^\infty I(q)q^2 \cos(qz)\mathrm{d}q}{\int_0^\infty I(q)q^2\mathrm{d}q} \qquad (3)$$

where z is parallel to the drawing direction. Multiplication of q^2 to $I(q)$ is necessary to account for the isotropic distribution of the crystalline lamellae in the selected systems prior to deformation.[1,47] The one-dimensional scattering intensity distribution of isothermally crystallized HDPE measured before deformation and the resultant correlation functions for the three populations of lamellar stacks are given in Figure 6. The scattering intensity distribution profile was decomposed into contributions from two populations of lamellar stacks based on Gaussian functions, as given in the top plot of Figure 6. The inset in the bottom plot demonstrates how the average thickness of the amorphous layers (d_a) and the long spacing (d_{ac}) were obtained.[1] It must be mentioned that it is impossible to decide whether it is the amorphous or the crystalline thickness that is read out from the correlation function without prior knowledge of crystallinity. However, the crystallinity of the sample used in the present study was higher than 0.5. Thus, the smaller value is assigned to the average thickness of the amorphous layers. As a result, the average thicknesses of the amorphous layers for lamellae I and lamellae II, and the quenched sample, are 15.6, 8.9, and 8.6 nm, respectively. A larger thickness of the amorphous layers implies a higher molecular mobility because the entangled amorphous phases between the lamellae are confined to a lesser extent. Accordingly, the sample with a more mobile amorphous phase exhibits a reduced modulus of the entangled amorphous network. The higher network mobility in the amorphous phase of lamellae I is ascribed to a significant reduction of concentration of tie-molecules connecting adjacent lamellae and an increase in the concentration of chain-ends. This is the consequence of the isothermal thickening of polyethylene crystalline lamellae

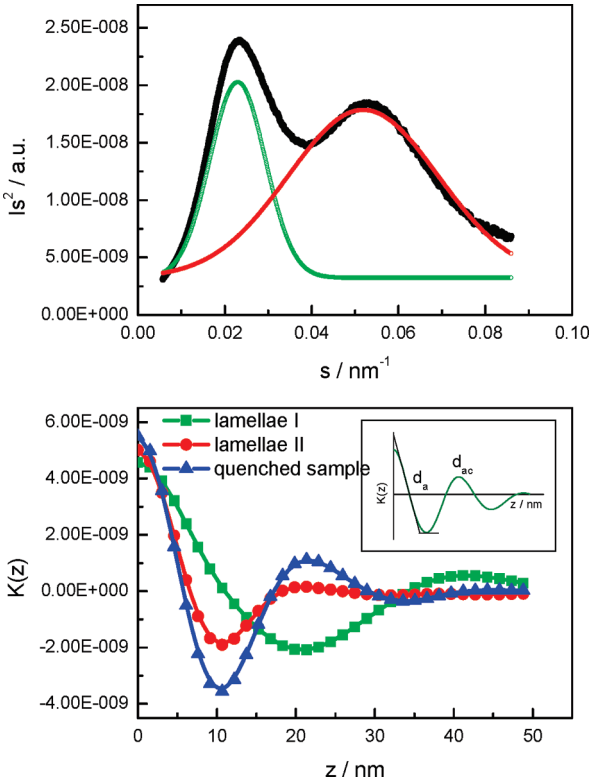

Figure 6. SAXS. One-dimensional scattering intensity distribution of isothermally crystallized HDPE along the stretching direction measured before deformation and the decomposition into two lamellar stack contributions (top), as well as the one-dimensional correlation function derived from the isothermally crystallized and quenched HDPE samples before deformation (bottom). The long spacing (d_{ac}) and the average amorphous layers thickness (d_a) can be obtained from the correlation function as illustrated in the inset of the bottom figure.

during isothermal crystallization.[45,53,54] Such an isothermal thickening is accompanied by the dissolution of a portion of crystallites resulting in eliminating tie chains previously connecting them and pushing more chain end cilia into the amorphous phase (cf. model presented in Figure 11 of ref 45). The resultant amorphous phase must exhibit a reduced effective network modulus because part of the entanglements including chain ends may easily be freed during deformation. On the other hand, the amorphous phase within stacks of thin lamellae grown upon cooling did not undergo such reorganization during fast crystallization. Combined with the assumption of a homogeneous strain distribution during deformation,[1,21,55] the differences in network moduli between the different amorphous phases can be employed to explain the existence of two critical strains when the isothermally crystallized sample is deformed. Since the amorphous network modulus of stacks of lamellae I was smaller than that of lamellae II, the stress generated in the stacks of lamellae I should be lower than that in lamellae II at a given imposed strain. Therefore, the critical stress, above which the crystalline blocks are no longer stable, is reached first for lamellae II at a smaller strain and then at a larger strain for lamellae I, giving rise to a two-step deformation process. Additionally, the critical strain for the quenched sample was equivalent to that observed for lamellae II, primarily due to their similar amorphous phase chain mobility.

4. Conclusions

The microstructural evolution of isothermally crystallized HDPE was investigated as a function of true strain using

scanning synchrotron SAXS experiments. It was found that in the process of lamellar to fibrillar transition, intralamellar slips of the crystalline blocks were activated at low deformations, followed by stress-induced fragmentation and a recrystallization process. Moreover, the role of the mobility of the entangled amorphous phase in the tensile deformation process was elucidated. A two-step deformation behavior can be observed when the isothermally crystallized sample was tensile deformed at 100 °C. This finding was ascribed to the sequential destruction of lamellae II and lamellae I due to different network moduli of the interlamellar amorphous phase. A quenched sample exhibited a similar critical strain as the one observed for lamellae II because of the comparable mobility of their amorphous phases.

Acknowledgment. We acknowledge financial support from National Natural Science Foundation of China (20734006, 50603024, and 50921062) and National Basic Research Program of China (2005CB623800) and HASYLAB project II-20080190.

References and Notes

(1) Strobl, G. *The Physics of Polymers*, 2nd ed.; Springer: Berlin, 1997.
(2) Failla, M. D.; Mandelkern, L. *Macromolecules* **1993**, *26*, 7167.
(3) Kennedy, M. A.; Peacock, A. J.; Mandelkern, L. *Macromolecules* **1994**, *27*, 5297.
(4) Butler, M. F.; Donald, A. M.; Bras, W.; Mant, G. R.; Derbyshire, G. E.; Ryan, A. J. *Macromolecules* **1995**, *28*, 6383.
(5) Butler, M. F.; Donald, A. M.; Ryan, A. *Polymer* **1997**, *38*, 5521.
(6) Young, R. J.; Bowden, P. B.; Ritchie, J. M.; Rider, J. G. *J. Mater. Sci.* **1973**, *8*, 23.
(7) Geil, P. H.; Ginzburg, B. M. *J. Macromol. Sci., Phys.* **2006**, *B45*, 291.
(8) Keller, A.; Pope, D. P. *J. Mater. Sci.* **1971**, *6*, 453.
(9) Pope, D. P.; Keller, A. *J. Polym. Sci., Polym. Phys. Ed.* **1975**, *13*, 533.
(10) Liu, L. Z.; Hsiao, B. S.; Fu, B. X.; Ran, S. F.; Toki, S.; Chu, B.; Tsou, A. H.; Agarwal, P. K. *Macromolecules* **2003**, *36*, 1920.
(11) Peterlin, A. *J. Mater. Sci.* **1971**, *6*, 490.
(12) Schultz, J. M. *Polymer Materials Science*; Academic Press: Englewood Cliffs, NJ, 1974.
(13) Lin, L.; Argon, A. *J. Mater. Sci.* **1994**, *29*, 294.
(14) Ward, I. *Mechanical Properties of Solid Polymers*; Wiley: New York, 1983.
(15) Men, Y.; Strobl, G. *Macromolecules* **2003**, *36*, 1889.
(16) Men, Y.; Rieger, J.; Lindner, P.; Enderle, H. F.; Lilge, D.; Kristen, M. O.; Mihan, S.; Jiang, S. *Polymer* **2007**, *48*, 2464.
(17) Jiang, Z. Y.; Tang, Y. J.; Men, Y. F.; Enderle, H. F.; Lilge, D.; Roth, S. V.; Gehrke, R.; Rieger, J. *Macromolecules* **2007**, *40*, 7263.
(18) Pawlak, A.; Galeski, A. *Macromolecules* **2005**, *38*, 9688.
(19) Ran, S. F.; Wang, Z. G.; Burger, C.; Chu, B.; Hsiao, B. S. *Macromolecules* **2002**, *35*, 10102.
(20) Tang, Y. J.; Jiang, Z. Y.; Men, Y. F.; An, L. J.; Enderle, H. F.; Lilge, D.; Roth, S. V.; Gehrke, R.; Rieger, J. *Polymer* **2007**, *48*, 5125.
(21) Men, Y.; Strobl, G. *Chin. J. Polym. Sci.* **2002**, *20*, 161.
(22) Young, P.; Stein, R. S.; Kyu, T. *J. Polym. Sci., Polym. Phys.* **1990**, *28*, 1791.
(23) Song, H. H.; Argon, A. S.; Cohen, R. E. *Macromolecules* **1990**, *23*, 870.
(24) Bowden, P. B.; Young, R. J. *J. Mater. Sci.* **1974**, *9*, 2034.
(25) Bartczak, Z.; Lezak, E. *Polymer* **2005**, *46*, 6050.
(26) Seguela, R.; Rietsch, F. *J. Mater. Sci. Lett.* **1990**, *9*, 46.
(27) Galeski, A.; Bartczak, Z.; Argon, A. S.; Cohen, R. E. *Macromolecules* **1992**, *25*, 5705.
(28) Flory, P. J.; Yoon, D. Y. *Nature* **1978**, *272*, 226.
(29) Juska, T.; Harrison, I. R. *Polym. Eng. Sci.* **1982**, *22*, 766.
(30) Popli, R.; Mandelkern, L. *J. Polym. Sci., Polym. Phys. Ed.* **1987**, *25*, 441.
(31) Wu, W.; Wignal, G. D.; Mandelkern, L. *Polymer* **1992**, *33*, 4137.
(32) Peterlin, A.; Meinel, G. *Makromol. Chem.* **1971**, *142*, 227.
(33) Meinel, G.; Peterlin, A. *Colloid Polym. Sci.* **1970**, *242*, 1151.
(34) Corneliussen, R.; Peterlin, A. *Makromol. Chem.* **1967**, *105*, 193.
(35) Men, Y.; Strobl, G. *J. Macromol. Sci., Phys.* **2001**, *B40*, 775.
(36) Men, Y. F.; Rieger, J.; Strobl, G. *Phys. Rev. Lett.* **2003**, *91*, 095502.
(37) Hiss, R.; Hobeika, S.; Lynn, C.; Strobl, G. *Macromolecules* **1999**, *32*, 4390.
(38) Hobeika, S.; Men, Y.; Strobl, G. *Macromolecules* **2000**, *33*, 1827.
(39) Al-Hussein, M.; Strobl, G. *Macromolecules* **2002**, *35*, 8515.
(40) Bartczak, Z. *Macromolecules* **2005**, *38*, 7702.
(41) Kiass, N.; Khelif, R.; Boulanouar, L.; Chaoui, K. *J. Appl. Polym. Sci.* **2005**, *97*, 272.
(42) Pawlak, A. *Polymer* **2007**, *48*, 1347.
(43) Wunderlich, B. *Macromolecular Physics*; Academic Press: New York, 1973; Vol. *1*.
(44) Montezinos, D.; Wells, D. G.; Burns, J. L. *J. Polym. Sci. Lett.* **1985**, *23*, 421.
(45) McCready, M. J.; Schultz, J. M.; Lin, J. S.; Hendricks, R. W. *J. Polym. Sci., Polym. Phys.* **1979**, *17*, 725.
(46) Stribeck, N. *X-ray Scattering of Soft Matter*; Springer: Heidelberg, 2007.
(47) Glatter, O.; Kratky, O. *Small-Angle X-ray Scattering*; Academic Press: London, 1982.
(48) Jiang, Z. Y.; Tang, Y. J.; Rieger, J.; Enderle, H. F.; Lilge, D.; Roth, S. V.; Gehrke, R.; Wu, Z.; Li, Z.; Men, Y. F. *Polymer* **2009**, *50*, 4101.
(49) Peterlin, A.; Baltá-Calleja, F. J. *Kolloid Z. Z. Polym.* **1970**, *242*, 1093.
(50) Murthy, N. S.; Bednarczyk, C.; Moore, R. A. F.; Grubb, D. T. *J. Polym. Sci., Polym. Phys.* **1996**, *34*, 821.
(51) Strobl, G.; Schneider, M. J. *J. Polym. Sci., Polym. Phys.* **1980**, *18*, 1343.
(52) Strobl, G.; Schneider, M. J.; Voigt-Martin, I. G. *J. Polym. Sci., Polym. Phys.* **1980**, *18*, 1361.
(53) Petermann, J.; Gleiter, H. *Colloid Polym. Sci.* **1976**, *254*, 247.
(54) Petermann, J.; Miles, M.; Gleiter, H. *J. Macromol. Sci., Part B: Phys.* **1976**, *12*, 393.
(55) Fu, Q.; Men, Y. F.; Strobl, G. *Polymer* **2003**, *44*, 1927.